International Journal of Humanoid Robotics
Vol. 9, No. 2 (2012) 1250009 (26 pages)
© World Scientific Publishing Company
DOI: 10.1142/S0219843612500090

HUMANOID LOCOMOTION PLANNING FOR VISUALLY GUIDED TASKS

JEAN-BERNARD HAYET[*,‖], CLAUDIA ESTEVES[†,**],
GUSTAVO ARECHAVALETA[†,††], OLIVIER STASSE[§,‡‡]
and EIICHI YOSHIDA[¶,§§]

[*]*Centro de Investigación en Matemáticas,*
CIMAT, Jalisco s/n. Col. Valenciana,
36240 Guanajuato, Guanajuato, México

[†]*Departamento de Matemáticas,*
Universidad de Guanajuato,
Jalisco s/n. Col. Valenciana,
36240 Guanajuato, Guanajuato, México

[‡]*Robotics and Advanced Manufacturing Group,*
Centro de Investigación y de Estudios Avanzados del IPN,
CINVESTAV, Saltillo, Coah, México

[§]*LAAS-CNRS,*
Laboratoire d'Analyse et d'Architecture des Systèmes,
Groupe Gepetto, 7, avenue du Colonel Roche,
31077 Toulouse Cedex 4, France

[¶]*CNRS-AIST, JRL (Joint Robotics Laboratory),*
UMI 3218/CRT, Intelligent Systems Research Institute,
AIST Central 2, Umezono 1-1-1, Tsukuba,
Ibaraki 305-8568 Japan
[‖]*jbhayet@cimat.mx*
[**]*cesteves@cimat.mx*
[††]*garechav@cinvestav.edu.mx*
[‡‡]*ostasse@laas.fr*
[§§]*e.yoshida@aist.go.jp*

Received 12 February 2011
Accepted 30 September 2011
Published 22 June 2012

In this work, we propose a landmark-based navigation approach that integrates (1) high-level motion planning capabilities that take into account the landmarks position and visibility and (2) a stack of feasible visual servoing tasks based on footprints to follow. The path planner computes a collision-free path that considers sensory, geometric, and kinematic constraints that are specific to humanoid robots. Based on recent results in movement neuroscience that suggest that most humans exhibit nonholonomic constraints when walking in open spaces, the humanoid steering behavior is modeled as a differential-drive wheeled robot (DDR). The obtained paths are made of geometric primitives that are the shortest in distance in free spaces. The footprints around the path and the positions of the landmarks to which the gaze must be directed are used within a stack-of-tasks (SoT) framework to compute the whole-body motion of the humanoid. We provide some experiments that verify the effectiveness of the proposed strategy on the HRP-2 platform.

Keywords: Nonholonomic motion planning; landmark-based navigation; humanoid motion generation.

1. Introduction

One of the first things to determine whether a humanoid robot is autonomous is its ability to navigate safely around obstacles. Several works during the past decade have tackled this important problem by using in general a two-stage algorithm: first, a motion planner computes a feasible collision-free trajectory for the robot focusing on the geometric, kinematic, and dynamic restrictions of the humanoid and its environment. In a second stage, the computed trajectory is executed, generally by using an open-loop control strategy.

In this work, we propose a two-stage landmark-based navigation strategy that, in addition to the geometric, kinematic, and dynamic restrictions, considers sensory constraints at the planning stage. Here, we focus on visual sensors and aim to ensure the visibility of visual landmarks in the environment. Landmarks play an important role to control the amount of uncertainty on the robot localization within a navigation framework. In this sense, our planner guarantees that at least one landmark in the environment will be visible to the humanoid at all moments of its navigation task. The problem of maintaining at least one landmark visible at all times while ensuring kinematic and dynamic feasibility is stated as a geometric problem of motion planning with equality and inequality constraints.

The main contributions of this work are:

- To state the landmark-based navigation problem as a motion planning problem that can deal with constraints of different natures (i.e., equalities and inequalities) which are specific to humanoid robots. These constraints appear at different levels in the proposed strategy.
- To provide a set of footprints that guarantee the visibility of at least one landmark and that take the humanoid robot from an initial to a goal configuration if the footprints were to be executed with no drift.
- To integrate and validate the whole strategy on a real humanoid platform.

The remaining of this work is organized as follows: in Sec. 2, we describe what we believe to be the most relevant works related to our approach. In Sec. 3, our overall strategy is depicted. In Sec. 4, we explain the different steps of the global path planner and the way the equality and inequality constraints are handled. Section 5 describes the whole-body motion synthesis strategy and the visual servoing task which guarantees the correct execution of the landmark-gazing task computed by the global planner. Section 6 shows experimental results, both in simulation and on the real humanoid robot HRP-2. Finally, in Sec. 7, we present our conclusions and future work for this proposal.

2. Related Work

During the past few years, several motion planners for humanoid robots have been proposed in the literature. In the same way as for any other mechanism, planners for humanoid robots can be local, which has the advantage that generated motions are more reactive, or global, which allows avoiding local minima. Both of these methods can integrate more or less easily equality or inequality constraints such as collision avoidance, verification of joint limits, and stability constraints. An overview of motion planning methods that deal with humanoid locomotion, mostly focusing on the planners experimented on the robot HRP-2, can be found in Ref. 1. Within these planners, it has been a common practice to use a global planner to ensure the feasibility of the desired task and then a local planner to generate and enforce locally the desired motion for the mechanism. For humanoid robots, this family of approaches have been proposed for different kind of tasks and constraints. For example, in Ref. 2, the authors propose a global planner for generating a set of individual footsteps that ensure the feasibility of the locomotion task in rough terrains. An online local pattern generator on the robot H7 enforces the task of following the planned footsteps. In Ref. 3, the global planner consists of three stages, where in the first, a coarse path for a simplified model of the robot is obtained and in the last, NBSP the footsteps for the local pattern generator are computed. A planner handling contact constraints for locomotion that can involve other parts of the humanoid body for additional stability has been proposed in Ref. 4. The global planner determines the type of contact and the position. The local planner, in the form of a numerical inverse kinematics (IK) solver, enforces the contact and closed kinematic chain constraints. Another multicontact constraints motion planner has been described in Ref. 5 where the authors have a global posture generator and then a local potential field function driving the motion from one posture to another. This planner has been implemented successfully on the HRP-2 platform. A global planner that also considers closed kinematic chains but for two-hand manipulation while walking is presented in Ref. 6. In that work, the authors use a nonholonomic reduced model of the humanoid to produce smooth collision-free trajectories for the robot and the object. The global planner outputs the footprints and the positions of both hands of the humanoid on the object. These local constraints are handled inside a redundant IK solver. In Ref. 7, the global planner outputs a smooth walking path with at the same time the grasping constraints for the humanoid to pivot a large box on a given environment. The kind of local planner used in all of these works, a prioritized stack-of-tasks (SoT) framework (e.g., Ref. 8), has become a common paradigm to use inside global planners for humanoid robots. These stacks usually include, as tasks with a high priority, collision avoidance or robot stability, and as tasks with lower priority, manipulation or visibility constraints, for example. In order to solve as many tasks in the stack as possible, the global planner is in charge of enabling or disabling tasks and changing their priorities (e.g., Refs. 9 and 10). In Ref. 11, the same task-priority redundancy formalism, this time based on the operational space, has been integrated as a local method embedded in a global motion planner for mobile manipulation tasks. This kind of planners integrating a global supervisor with a local stack of tasks have already proven to be effective on real experimentation as for example in Refs. 12 and 13. In Ref. 13, visual constraints were integrated within the tasks that had to be solved in the stack. In Ref. 14, visual constraints are also handled locally for the task of grasping an object while walking within the stack of tasks. In our previous work,[15] we have introduced a global motion planner that considers visibility constraints from a global perspective. In this way, the feasibility of the visual task together with the navigation task can be ensured and, in a local manner, both of these tasks are enforced. In the present paper, our contribution relative to Ref. 15 is the possibility of ensuring the visibility of at least one landmark among many during all the length of the path. In addition, we have tested our algorithm experimentally on the humanoid robot HRP-2.

3. Proposed Approach

In this work, we propose a motion planner that computes whole-body collision-free walking trajectories for a humanoid robot with the constraint of keeping at least one landmark in sight during all the trajectory. The planner is divided into several stages:

(I) First, a global motion planner (see Sec. 4) computes a collision-free path for a reduced model of the system. As a reduced model for the humanoid robot navigating in large environments, we have proposed a differential-drive wheeled robot (DDR). This choice has been done based on recent results in the community of Movement Neuroscience,[16] suggesting that most humans exhibit nonholonomic constraints when walking in open spaces.[17] The DDR model is coupled with a limited field-of-view sensor attached to it. Then, the planner computes a collision-free path taking into account the sensor limitations to keep at least one landmark within its field of view during the path at all times. At the end of this stage, the robot gazing profile for the sensor and its footprints is extracted from the path by considering the robot step length and width.

(II) Footsteps are then converted into dynamic stable biped locomotion of humanoid through a walking pattern generator. We adopt a method based on the preview control for ZMP[18] for this conversion. This method computes a trajectory for the ZMP from footsteps (position and orientation) to obtain the humanoid center of mass (CoM) reference trajectory for walking motion. This CoM reference trajectory is obtained by a control system based on the cart-table reduced model presented in Ref. 18. The whole-body motion is generated at execution time with a local method based on an SoT approach (see Sec. 5) where the task of gazing at the landmark is supervised by a visual servoing module that is projected into the null space of the locomotion task.

The following sections elaborate on each of these stages.

4. Global Path Planner

Given the modeling of the whole humanoid robot as a DDR, we describe here how to plan 2D trajectories to ensure visibility of at least one landmark all along the computed path. First, we describe precisely the simplified model (Sec. 4.1) and the constraints that are associated to it. Then, we detail the planning algorithm whose overall strategy is described in Fig. 1, which corresponds to our global planner for the simplified model (detailed in Sec. 4.3). The blocks in Fig. 1 represent each of the main steps in our strategy and the section of the paper in which they are described. This planner takes as input the initial and final locations desired for the robot as well as a geometric description of the environment and the landmarks' positions. Then, a global path is formed recursively by using at each step the synthesis of locally optimal paths (described in Sec. 4.2). From this procedure, a 2D path, resulting from the concatenation of locally optimal subpaths, is obtained. The output of this strategy are the footprints extracted from this 2D path (Sec. 4.4), which are used to plan the motion for the whole humanoid and the landmark that the robot has to maintain in view at each step of the path.

4.1. *Simpliffed model description and constraints*

The differential-drive simplified model is composed by a subset of the underactuated degrees of freedom of the humanoid kinematic structure. We will denote them by $\mathbf{q}_{\text{ddr}} = (x, y, \theta)^T \in SE(2) = \mathcal{C}_{\text{ddr}}$ (the configuration of the differential-drive simplified model), where (x, y) is the position of the robot on the plane and θ its orientation. We also introduce ϕ, the angle that the sensor makes with respect to the robot

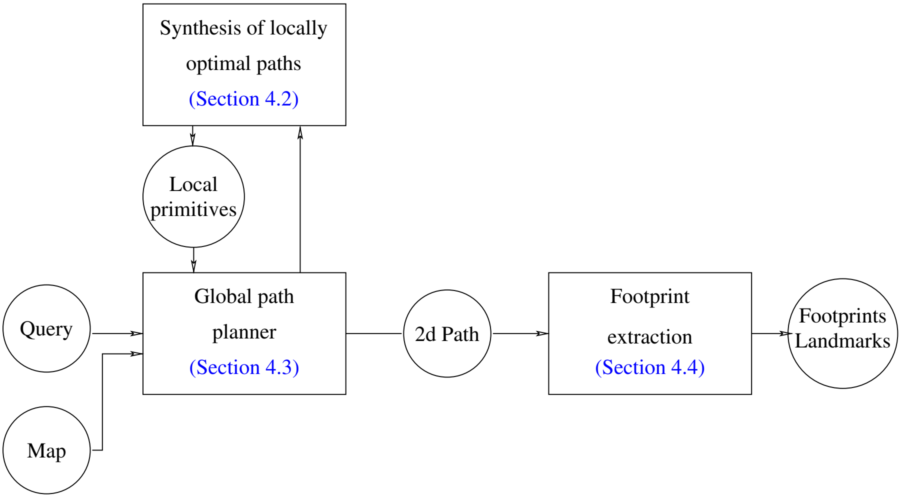

Fig. 1. Global planning strategy for the simplified model: the global planner relies locally on optimal paths synthesis and outputs a 2D path from which a set of footprints and a set of landmark positions (the ones the robot will direct its gaze to) are extracted.

orientation. It is not a degree of freedom *per se*, as its value is constrained by the presence of the landmark at the center of the field of view. It should be noted that all the coordinates are relative to the position of the landmark which is currently guiding the robot. This model may capture the human-like walking behavior, provided that several constraints expressed on the configuration space $\mathcal{C}_{\text{ddr}}$ of the reduced model can be satisfied:

- The human-like walking behavior is characterized by an equality constraint on the tangent bundle of $\mathcal{C}_{\text{ddr}}$, i.e. the nonholonomy equation (Eq. (1)):
$$\dot{x}\sin\theta - \dot{y}\cos\theta = 0. \tag{1}$$
- The landmark visibility gives rise to an equality constraint on $\mathcal{C}_{\text{ddr}}$ that links the polar angle corresponding to the robot position, the orientation of the robot, and the sensor angle ϕ. These constraints are written in Eq. (2):
$$\theta = \arctan\left(\frac{y}{x}\right) - \phi + (2k+1)\pi, \quad k \in \mathbb{Z}. \tag{2}$$
- The sensor limits can be translated into simple inequalities on the sensor angle, ϕ, by defining bounds (ϕ^-, ϕ^+) such that:
$$\phi^- \leq \phi \leq \phi^+.$$
- Lastly, the polygonal obstacles in the environment generate inequality constraints in $\mathcal{C}_{\text{ddr}}$ of two kinds: By causing direct collision with the robot or by generating shadows for the landmark visibility.

As it has been shown recently, it is possible (1) in the absence of obstacles to give an analytical expression for shortest length trajectories while handling the first three constraints (nonholonomy, landmark visibility, and sensor angular limits and (2) in the presence of obstacles to plan collision-free trajectories based on the optimal ones without obstacles, through a recursive, complete scheme. The following paragraphs partly recall the results from recent works in the area[19–21] and extend them in several ways.

4.2. *Synthesis of locally optimal paths*

In the absence of obstacles, the optimal trajectories for such a system under the first three constraints above (nonholonomy, landmark visibility, and sensor limits) have been shown to be sets of at most four pieces of segments of logarithmic spirals (referred to as "S"), segments of straight lines (referred to as "L"), and in-site rotations (referred to as "R").[19,21] Logarithmic spirals are those curves that maintain the sensor angle ϕ to a saturated value, so that there are two possible spirals at one point: S^+ (in which $\phi = \phi^+$) and S^- (in which $\phi = \phi^-$). In open spaces, these paths are optimal in terms of Euclidean distance, that is, they minimize:
$$\mathcal{P}^* = \min_{\mathcal{P}} \mathcal{C}(\mathcal{P}), \tag{3}$$
where $\mathcal{C}(\mathcal{P}) = \int_{\mathbf{P}_i}^{\mathbf{P}_f} \mathrm{d}s$ and s is the curvilinear abscissa along $\mathcal{P}$.

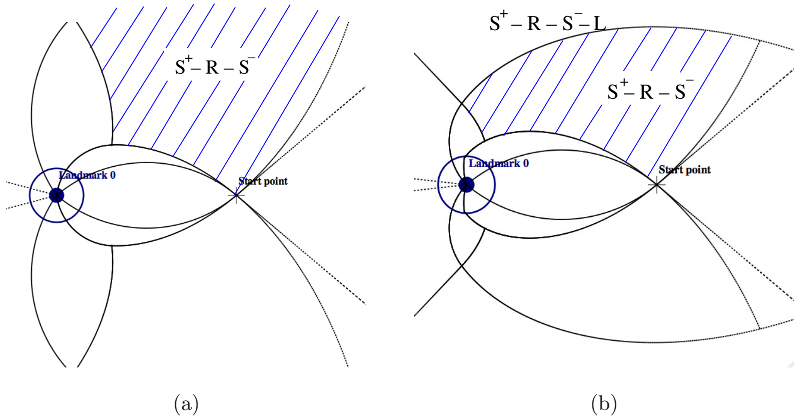

(a) (b)

Fig. 2. Shortest path synthesis for DDRs maintaining a landmark in sight for $Q = 1$ (left) and $Q \approx 2.3$ (right). Each of the region delimited by black curves corresponds to a different kind of shortest trajectory, made of pieces of logarithmic spirals S^+ or S^-, straight lines L, and in-site rotation R. The criterion which is optimized here is the one of Eq. (4). Note that the regions where a spiral has to be done backward (e.g., the one above the starting point, $S^+ - R - S^-$) are reduced in favor of the ones where the backward part is done in straight line ($S^+ - R - S^- - L$).

A full synthesis of these optimal paths has been described in a recent work.[21] For any pair of initial and final configurations $\mathbf{P}_i$ and $\mathbf{P}_f$, it gives the sequence of primitives to execute. We will partly rely on it for the subsequent steps of our algorithm. This synthesis is illustrated by Fig. 2 (left). It depicts, for one starting position and one landmark position, the partition of the plane according to the nature of the shortest path to be done to reach the final point, which can be chosen anywhere in the plane. An example of a path obtained by this synthesis is given as the red path (light gray) in the upper part of Fig. 3, which is made of four nonzero length primitives.

One of the most noticeable characteristic of the paths computed as described above is the juxtaposition of segments of trajectories that move forward and segments that move backward. However, for humanoid robots, *backward motion should be minimized* when possible, as backward motion is generally more insecure, since no sensor feedback allows to detect obstacles, for example. We describe hereafter a first way to penalize backward motion, by modifying the criterion $\mathcal{C}$ from Eq. (3).

The new criterion $\mathcal{C}'(\mathcal{P})$ is defined over the set of possible paths $\mathcal{P}$ starting at $\mathbf{P}_i$ and ending at $\mathbf{P}_f$, as follows:

$$\mathcal{C}'(\mathcal{P}) = \int_{\mathbf{P}_i}^{\mathbf{P}_f} q(s)\mathrm{d}s, \tag{4}$$

where,

$$q(s) = \begin{cases} 1 & \text{if } \dot{x}(s)\cos\theta(s) + \dot{y}(s)\sin\theta(s) > 0, \\ Q & \text{if } \dot{x}(s)\cos\theta(s) + \dot{y}(s)\sin\theta(s) < 0, \end{cases}$$

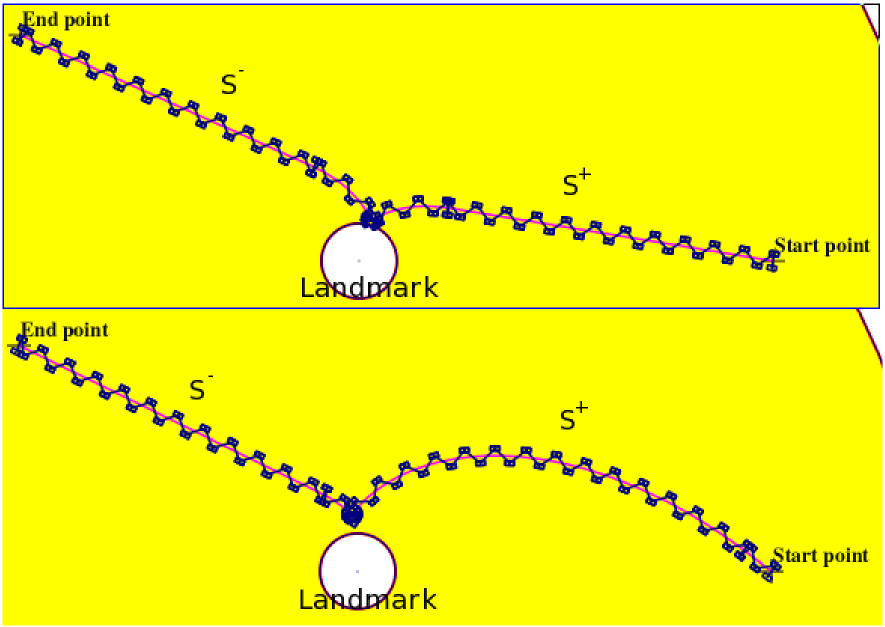

Fig. 3. Effect of the penalizing term Q on the motion primitives for the synthesis of shortest paths. In both cases, the same request is entered, for $Q = 1$ above and $Q > 1$ below. Both of the optimal trajectories are of the type $L - S^+ - R - S^- - L$, but in the case below, the backward part tends to reduce to the straight line part. In dark blue, footprints are generated from the computed trajectory.

and where $Q > 1$ is a constant term penalizing backward motion, which acts as a parameter of the algorithm.

The extension of the optimality results to the criterion $\mathcal{C}'(\mathcal{P})$ of Eq. (4) instead of the Euclidean distance is straightforward, as the factor Q only affects: (1) the spatial distribution of the nature of optimal curves and (2) the parameters of the curves involving both backward and forward motion. We spare the algebra to the reader and give the resulting plane partition (i.e., the path synthesis), for some $Q > 1$, in Fig. 2 (right). As an example, the stripped region on the figure is the one where $S^+{-}R{-}S^-$ trajectories are the shortest. On the right, the stripped region is reduced in favor of the $S^+ - R{-}S^- - L$ region, i.e. the backward spiral tends to be replaced by a smaller part under $\mathcal{C}'(\mathcal{P})$.

To further illustrate the effect of Q, we give in Fig. 3 two examples of optimal trajectories, without obstacles, for the same pair $(\mathbf{P}_i, \mathbf{P}_f)$. The upper one is the $L - S^+{-}R{-}S^-{-}L$ trajectory obtained for $Q = 1$, and the lower one is the trajectory *of the same type* obtained for $Q > 1$. Note that the first part of the trajectory (straight line, then spiral S^+) is done *forward*, whereas the second part (spiral S^-, then straight line) is done *backward*. One can observe that the effect of Q is to reduce the backward part to a simple straight line.

4.3. *Global path planner*

In this part, we use the results that we have stated above (that hold in the absence of obstacles) to propose a planning algorithm that handles obstacles (Sec. 4.3.1). Then, we generalize this algorithm to handle several landmarks (Sec. 4.3.2).

4.3.1. *Planning among obstacles*

In a recent work,[20] we have proposed a planning strategy to generate collision-free paths among obstacles and with the same constraints as before, i.e. that the landmark has to be kept in sight. The algorithm is described in the next few paragraphs.

The idea is to use a recursive scheme proposed in a previous work on car-like systems[22] and adapt it in order to cope with the landmark visibility constraints. Indeed, one of the effects induced by the presence of the landmarks is that they may generate *shadows* where the visibility is broken. Hence, to get the free space $\mathcal{C}_{\mathrm{ddr}}^{\mathrm{free}}$, not only the obstacles dilated by the robot shape (that we will suppose circular) have to be removed from the configuration space $\mathcal{C}_{\mathrm{ddr}}$ but also the shadows generated by them. Such an explicit building of $\mathcal{C}_{\mathrm{ddr}}^{\mathrm{free}}$ is illustrated in Fig. 4, and it is the first step of our algorithm. In the image at the right of Fig. 4, we show in blue $\mathcal{C}_{\mathrm{ddr}}^{\mathrm{free}}$ including the dilated obstacles, the shadows from the visibility computation from the landmark and the range limitations of the robot sensor. It should be noted that if the landmark lies on top of an obstacle, that portion of $\mathcal{C}_{\mathrm{ddr}}^{obst}$, the obstacle configuration space, would be the union of the dilated zone from the obstacle and the range limits of the landmark.

Then, by computing a roadmap on this representation of $\mathcal{C}_{\mathrm{ddr}}^{\mathrm{free}}$, we can easily obtain a feasible path for an equivalent point-like *holonomic* system. Steps 1 and 2 of Algorithm 1 hereafter reach this goal and capture the connectivity of the free space $\mathcal{C}_{\mathrm{ddr}}^{\mathrm{free}}$ with a *generalized Voronoi graph* (GVG) $\mathcal{G}$ for a circular robot *without considering its orientation* (i.e., in $\mathbb{R}^2$). Physical obstacles are dilated and merged to the aforementioned shadows. Then (in Step 4 of the algorithm), we try to connect the initial and final configurations $\mathbf{P}_i$ and $\mathbf{P}_f$ by using the optimal primitives given by the synthesis. If a collision is found in the newly generated path, it is split recursively

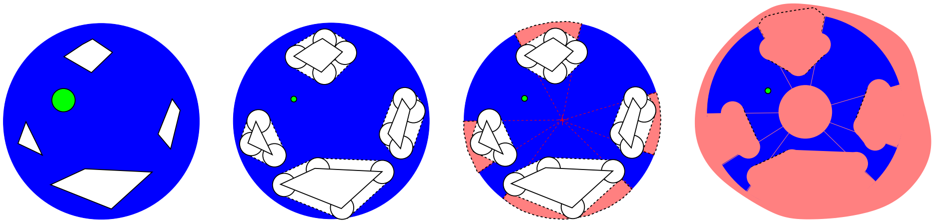

Fig. 4. Construction of $\mathcal{C}_{\mathrm{ddr}}^{\mathrm{free}}$ in the (x, y, ϕ) space. By dilating physical obstacles in the xy plane to define collision obstacles (white), the circular robot can be reduced to a point (green). Shadows and visibility constraints (Eq. (2)) define visibility obstacles (third from left).

```
Algorithm 1 Path planning of the DDR reduced model, one landmark
Require: Initial and final configurations $\mathbf{P}_i$ and $\mathbf{P}_f$. Landmark position $\mathbf{L}$.
Ensure: Footprints along a collision-free path $\mathcal{P}$ maintaining the landmark in sight.
1: Build an explicit representation of $\mathcal{C}_{\mathrm{ddr}}^{\mathrm{free}}$ as the difference of $\mathcal{C}_{\mathrm{ddr}}$ and the union of the dilated obstacles with the shadows induced by the landmark visibility;
2: Build the GVG $\mathcal{G}$ on $\mathcal{C}_{\mathrm{ddr}}^{\mathrm{free}}$; $\mathcal{C}_{\mathrm{ddr}}^{\mathrm{free}}$ being made of parts of lines or circles, $\mathcal{G}$ is made of parts of lines, parabolas or hyperbolas;
3: Given a starting and a goal configurations $(\mathbf{P}_i, \mathbf{P}_f)$, compute a path $\hat{\mathcal{P}}$ for the *holonomic* system associated to the robot by connecting these locations to $\mathcal{G}$; if not possible, *no nonholonomic path can be found as well*;
4: Recursively connect the starting and ending points with the optimal primitives; if the computed sub-paths are in collision, use the point at middle-path in $\hat{\mathcal{P}}$ as a sub-goal and re-apply the recursive procedure to the two resulting sub-paths;
5: *Optimize* the final path:
6: for $i = 1$ to $n_i$ do
7:     Generate $n_s$ randomly possible shortcuts between the constitutive primitives of the trajectory and apply the one that improves $\mathcal{C}(\mathcal{P})$;
8: end for
9: Transform the resulting path *into a set of footprints* for the humanoid robot, i.e., into sets of left and right feet positions (see Sec. 4.4).
```

Algorithm 1. Path planning of the DDR reduced model, one landmark.

into pieces, such that each piece is replaced with a shortest path between the previously initial or final configurations and the split point. It should be noted that at this stage the generated collision-free path is not optimal in distance but each piece is locally optimal. As it can be guessed, the algorithm is most efficient when the clearance from the obstacles in the original roadmap is maximized[23,22] as the number of subdivisions will be inferior. The GVG gives the roadmap that maximizes this clearance. It can also be proven[24] that this subdivision procedure will stop at a certain length of the subpaths, which is a function of the distance from the robot to the closest obstacle.

Step 4 of Algorithm 1 produces feasible collision-free paths which are likely to have useless detours and maneuvers (the shortest length paths in the presence of obstacles are going to be in contact with the obstacles and therefore not collision-free and insecure for a humanoid robot to execute). An efficient and very simple strategy to implement for path optimization is to take two random points from the feasible path of Step 4 and try to replace the subpath in-between the two configurations with a shortest-length primitive from the synthesis. If the subpath is collision-free and if it is not of the same length as the previous path, it will be necessarily of a shorter length and can therefore replace the original segment. This procedure is performed until, after a given number of tries, no new collision-free length-reducing subpath is found.

This optimization strategy does not compromise the completeness of the overall algorithm.

This algorithm converges and is complete for the DDR reduced model, in the sense that it will give a trajectory if and only if there is an existing one. Details on the implementation can be found in our previous work,[20] in particular the way the GVG edge weights can be set in such manner that either the shorter or safer paths can be preferred.

A contribution to this algorithm, not present in our previous works,[20,24] is that in order to further penalize backward motion, we set weights in the edges $\mathcal{E}$ of the GVG $\mathcal{G}$ that depend on (1) the *length* of the arcs corresponding to this edge, (2) the *clearance* along the arc, and (3) the proportion of the path that would have to be done backward between the two end points of the arc, if no obstacles were present. The combination of these factors is done in a heuristic way as:

$$w(\mathcal{E}) = \min(\mu, f(\mathcal{E}))\frac{l(\mathcal{E})}{1+\gamma c(\mathcal{E})},$$

where $l(\mathcal{E})$ is the length of the edge, $c(\mathcal{E})$ the minimal clearance along $\mathcal{E}$, and $f(\mathcal{E}) \in [0,1]$ is the ratio of the path along the edge that is done backward. The constants $\mu > 0$ and γ are user-defined and allow to emphasize one factor over the others. A comparison between two path with and without the term in $f(\mathcal{E})$ in the graph weights is shown in Fig. 5.

Humanoid robots are expected to work on human populated environments. If a moving obstacle, such as a person traversing the robot working area, is found while the robot executes its path, two different strategies can be followed:

(1) If the moving obstacle is blocking the computed trajectory, the robot can stop or reduce its velocity depending on the distance to the obstacle and wait for the obstacle to pass.
(2) If the moving obstacle is not blocking the robot path but occluding the landmark, the robot continues performing its trajectory keeping an estimate of the

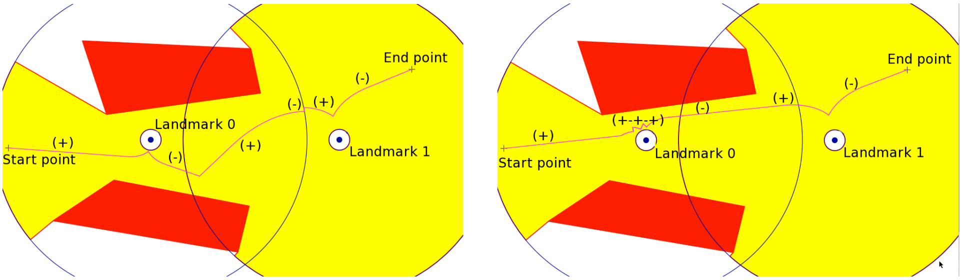

Fig. 5. Including the proportion of forward motion into the graph weights: on the left, the answer to a query that does not include this criterion; on the right, the answer to the same query with the criterion taken into account. In both cases, each primitive is labeled with a (+) for forward motions or with a (−) for backward motion. Overall, the proportion of the path being done backward is reduced.

landmark position. When the obstacle passes and the landmark is seen again, this estimate is corrected.

If the moving obstacle remains blocking the path or occluding the landmark for a given time interval, it is included to the robot map and a new path is computed.

These strategies are not currently integrated into our planning algorithm but they will be implemented as future work.

4.3.2. *Handling several landmarks*

Our next improvement upon the preliminary version of this work[15] has been the generalization of the previously mentioned method to the case of several landmarks, which is more extensively discussed in Ref. 24. This has been done in such a way that, along the generated path, at least one landmark remains visible at all times. Because of this, navigation is facilitated in the sense that, as the computed paths are followed, we can be sure in advance that landmarks can be relied on for visual localization. The implemented idea, more extensively detailed for the DDR model in a recently submitted paper,[24] is to generate a set of different roadmaps as shown above, for each landmark $\mathbf{L}_k$, and in which the same process as in Algorithm 1 is applied. Now, the difference is that for each pair of landmarks $(\mathbf{L}_k, \mathbf{L}_l)$, we also compute geometrically the subset of $\mathbb{R}^2$ where a switch of the gaze from landmark $\mathbf{L}_k$ to $\mathbf{L}_l$ is safe, i.e. where both are visible and none of them is lost while switching from one to the other. A set of nodes is extracted from the GVGs of these regions that allow the different individual roadmaps to be connected. As a result, we obtain a forest covering the union of the visibility areas for each landmark, and we use it in the same way as described above to generate collision-free paths. The algorithm is summed up in Algorithm 2.

An example of the steps and results of this extended algorithm is depicted in Fig. 6. First, in Fig. 6(a), the polyhedral environment with its obstacles and a set of three landmark visibility regions covering it are shown. Then, the union of the

```
Algorithm 2 Path planning of the DDR reduced model, several landmarks.
Require: Initial and final configurations $\mathbf{P}_i$ and $\mathbf{P}_f$, a set of landmarks $\mathbf{L}_k$.
Ensure: Footprints along a collision-free path $\mathcal{P}$ maintaining *at least* one landmark
    in sight and the sequence of corresponding landmarks to observe.
Build $\mathcal{C}^{\mathrm{free}}_{\mathrm{ddr},i}$ and a roadmap (GVG) $\mathcal{G}_i$ for each landmark $i$ as described in
    Algorithm 1.
Determine geometrically the sets $\mathcal{S}_{kl}$ where both landmarks $\mathbf{L}_k$ and $\mathbf{L}_l$ are visible
    and where a switch from gazing at one from the other is possible. Connect the
    GVGs $\mathcal{G}_i$ through the nodes of the GVGs of $\mathcal{S}_{kl}$.
Apply the recursive algorithm of Algorithm 1, optimize the solution if it exists
    and generate footprints.
```

Algorithm 2. Path planning of the DDR reduced model, several landmarks.

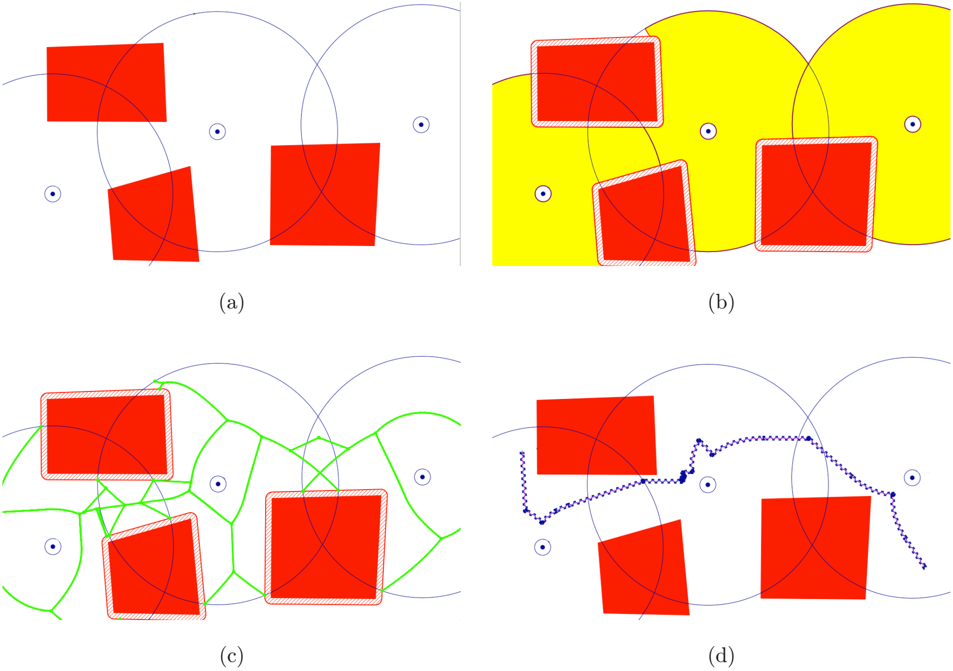
(a)
(b)
(c)
(d)

Fig. 6. Computing path among obstacles observing at least one landmark among several ones. Landmarks are depicted as dark dots. The final nonholonomic path is made of nontrivial primitives (pieces of lines or spirals) and in-site rotations: (a) Environment: obstacles and landmarks, (b) Visibility areas and dilated obstacles, (c) Computed and connected GVGs, and (d) Computed path and generated footprints.

visibility areas is shown in Fig. 6(b), and the graph resulting from the union of individual roadmaps, as described above, is shown in Fig. 6(c). Connector nodes, which connect individual roadmaps, are easily recognizable. Lastly, Fig. 6(d) shows the computed path resulting for a particular query and the footprint generation, explained hereafter, computed on it.

4.4. *Footprint extraction*

Once a path has been computed through Algorithm 2, the next step is to produce a set of footprints that will serve as input for the locomotion controller. We used a purely geometrical way to do so: given the specification of the humanoid robot (interfeet distance and desired step length, in particular), we first set the feet aligned with the initial configuration and then generate the different steps until a given distance from the end of the current part trajectory is attained (i.e., we stop the robot at nondifferentiable points to perform in-site rotations).

5. Local Whole-Body Motion Generator

As a local motion planner, we have used the method proposed in Ref. 14. To generate the whole-body motion of the humanoid robot, the first step is to obtain, from the footsteps extracted from the global planner, the desired stable trajectory of the CoM of the robot. This stable trajectory is used in a second step as the highest priority task inside the SoT formalism proposed in Ref. 14 and that we use here to enforce the visibility and geometric constraints that we know to be feasible because of the global planner of Sec. 4. The local method is able to generate dynamically stable biped walking motion that always maintains the ZMP inside the support polygon formed by the robot foot or feet.

5.1. *Pattern generator*

This method uses the locomotion pattern generator from Ref. 18 whose input is a set of footprints compliant with the robot stepping parameters, as in this case the footprints resulting from the global VDDR planner from Sec. 4. From these set of footsteps and the stepping period, the ZMP reference trajectory is derived and tracked using a preview control of a simplified 3D linear inverted pendulum. The real multibody dynamics of the robot are considered within a second stage of the preview controller to obtain a more accurate trajectory of the CoM. The CoM reference trajectory is the output of the pattern generator.

5.2. *Stack of tasks*

The local whole-body motion generator is a hierarchical IK solver as proposed in Ref. 14. Here, only two behaviors are involved in the local motion generation: locomotion and visual constraints enforcement. The main idea is to use the redundancy formalism[25,26] to compute a control law using a series of tasks, the one with the least priority projected into the null space of the one with one level above of priority and so on, until the highest level of priority is reached.

A kinematic task is represented by an error function $\mathbf{e}(\mathbf{q}) = \mathbf{x}_d - f(\mathbf{q})$, where $\mathbf{x}_d \in \mathbb{R}^m$ stands for the desired operational location in an m-dimensional space (i.e., position and orientation); $\mathbf{q} \in \mathbb{R}^n$ is the robot configuration in an n-dimensional configuration space; and $\mathbf{x} = f(\mathbf{q})$ is either a point or a location attached to the robot expressed in terms of its configuration. The exponential convergence of $\mathbf{e}(\mathbf{q})$ is achieved by means of $\ddot{\mathbf{e}}(\mathbf{q}) = -\alpha\mathbf{e}(\mathbf{q})$ where the linear system of equalities:

$$J(\mathbf{q})\dot{\mathbf{q}} = -\alpha\mathbf{e}(\mathbf{q}) \tag{5}$$

is satisfied, with $J(\mathbf{q}) \in \mathbb{R}^{m\times n}$ being the Jacobian of the task. Thus, when $m < n$, a hierarchical structure of tasks under the form $\{\mathbf{e}_1(\mathbf{q})\ \mathbf{e}_2(\mathbf{q})\ \ldots\ \mathbf{e}_p(\mathbf{q})\}$ can be defined on the $(n - m)$-dimensional null space. It contains p tasks ordered with decreasing priority, where to each task i is associated a Jacobian $J_i(\mathbf{q})$. The problem to be solved recursively for all $\mathbf{e}_i(\mathbf{q})$ is then formulated as:

$$\begin{aligned} &\min_{\dot{\mathbf{q}}_i \in \mathbb{R}^n, \mathbf{w} \in \mathbb{R}^m} && \frac{1}{2}\|\mathbf{w}\|^2 + \frac{1}{2}\|k_i \dot{\mathbf{q}}_i\|^2, \\ &\text{s.t.} && J_i(\mathbf{q}) Q_{i-1}(\mathbf{q}) \dot{\mathbf{q}}_i - (\ddot{\mathbf{e}}_i(\mathbf{q}) - J_i(\mathbf{q}) \dot{\mathbf{q}}_{i-1}) = \mathbf{w}, \end{aligned} \tag{6}$$

where $\dot{\mathbf{q}}_i$ are the successive versions of the vector of velocities and k_i a scalar controlling the regularization on the vector of velocities (see after). The matrix $Q_l(\mathbf{q}) = (I - J_l^+(\mathbf{q}) J_l(\mathbf{q})) \in \mathbb{R}^{n \times n}$ stands for the orthogonal projection of $J_l(\mathbf{q})$ and $J^+ = J^T (J J^T)^{-1}$ is the Moore–Penrose inverse of matrix J. This means that $J(\mathbf{q})$ and $Q(\mathbf{q})$ are orthogonal complements. The solution of Eq. (6) is given by the following recursive computation of the articular velocity as proposed in Ref. 25:

$$\begin{cases} \dot{\mathbf{q}}_0 = 0 \\ \dot{\mathbf{q}}_i = \dot{\mathbf{q}}_{i-1} + \widehat{J}_i(\mathbf{q})^{+k_i} (\ddot{\mathbf{e}}_i - J_i(\mathbf{q}) \dot{\mathbf{q}}_{i-1}), \quad \text{for } i = 1, \ldots, p \end{cases} \tag{7}$$

where $\widehat{J}^{+k} = J^T (J J^T + k^2 I)^{-1}$ is a singularly robust pseudo-inversion of J, with a factor k regulating this operation.[26] In our work, the tasks with the highest priorities are related to the locomotion behavior by specifying the position of both the feet and the CoM reference trajectory to be reached. The task Jacobian of the CoM is computed as in Ref. 27. As all of the DOFs of the humanoid lower body, including the underactuated DOFs, are used for locomotion, only those of the upper body remain available for defining additional tasks, in this case the enforcement of visual constraints. Inside the visual enforcement task, three subtasks are included:

(1) A *visual servoing* task, the goal of which is to minimize the error between the current value of the ith landmark (position of which is given as input by Algorithm (2) and the desired value resulting from the VDDR planner.
(2) A *centering* task to center the landmark in the image and stabilize the camera motion.
(3) A *joint limit avoidance* task.

In Sec. 4, it is explained that the paths obtained with the VDDR model are paths where the visual sensor is saturated. When we apply this to the humanoid robot, we profit from the upper body redundancy to avoid joint saturation by using the neck, chest, and waist degrees of freedom for keeping the landmark in sight.

More details on how to compute each of these tasks can be found in Ref. 14.

6. Experimental Results

In this section, we present some results of applying our strategy, first on simulations, then through two scenarios with the humanoid robot HRP-2 from the Joint French–Japanese Robotics Laboratory at Tsukuba. In all the experiments below, the planning part following the algorithms presented in Sec. 4.3 has been implemented in C++ with widespread software libraries. In particular, the Computational Geometry

Algorithms Library (CGAL) library was used for the 2D planner from which we benefited in particular to implement Voronoi diagrams.

6.1. *Simulations*

In this series of simulations, we used the pattern generation, including dynamics simulation and motion controllers, from the Open-HRP platform,[28] and our own implementation of IK for orienting the robot toward the landmark.

In a first scenario (first row of Fig. 7), we computed a feasible path (which is optimal), with one landmark to maintain in sight and without obstacles using all the elements described in Sec. 4. On the left side, the computed 2D path is shown, with the generated footprints in dark blue and the Voronoi diagram in blue. On the right

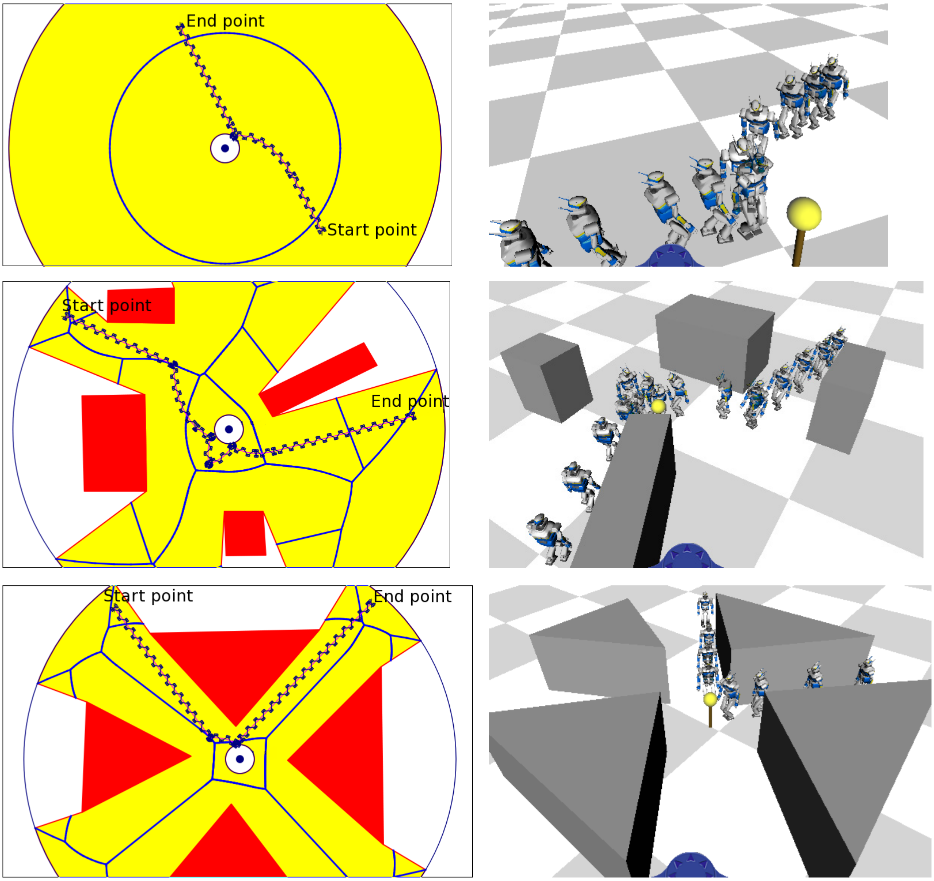

Fig. 7. Three examples of scenarios with (second and third rows) or without (first row) obstacles. The left column shows, in all cases, the trajectories computed by the 2D planner that allows for sensor restrictions to be met all along the trajectories. The spiral and line parts are quite distinguishable; the blue structures are the edges of the underlying GVG. The right column displays several configurations of the real trajectory performed by the humanoid. The landmark is represented by a yellow ball.

side, the trajectory made by the simulated robot is shown, with the landmark represented by the yellow sphere. Notice how the robot keeps the landmark in sight during the whole motion, which could be an important element in surveillance tasks, for example.

On the second and third rows, two other scenarios are depicted, with still one landmark to maintain in sight but this time including a set of polygonal obstacles which have to be avoided by the robot. Because of the algorithm design, the collision avoidance is done for a bounding cylinder around the robot, so that no 3D collision avoidance has been explicitly done. As in the previous case, the 2D path image shows the footprints computed around the obstacles as well as the Voronoi diagram for each of the environments. Note how the final footprints path has some of its intermediary points on the Voronoi diagram, which correspond to the recursion steps in the Algorithm 2 planning paths among obstacles. Again, in the right column, we show the simulated trajectory for the virtual humanoid robot. Figure 8 shows a close-up of some configurations near the landmark with the robot gaze directed to it.

The one-landmark scenarios of Figs. 7 and 8 have already been presented in Ref. 15. Here, they are presented to have a complete panorama of the results obtained with our algorithms for one and several landmarks.

A second scenario, this time with two landmarks, is shown in Fig. 9. The top row on this figure shows the initial and final configurations given as input to compute the path. The global path is constructed recursively using Algorithm 2 in order to ensure the visibility of at least one landmark (yellow spheres) at all times. The second and third rows of Fig. 9 show two configurations near the first landmark (a close-up on the left and a view of the complete environment on the right) where the robot has to maneuver to go around the landmark without losing sight of it. These maneuvers could eventually be changed into a different walking pattern for the humanoid robot, i.e. it could be executed using side steps, a pattern which we did not explore on the present work. The fourth row in Fig. 9 shows the moment where the switching of landmarks is executed. These motions depend on the amplitude of the viewing field of the simulated robot. The figure on the left shows the moment when the robot is able to see both landmarks and the figure on the right shows when the robot has already switched from one landmark to the other. In the bottom row of Fig. 9 (left), a

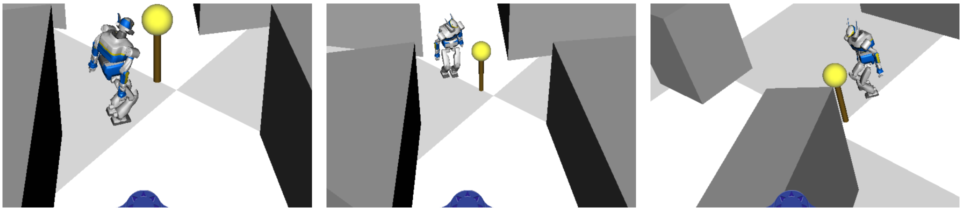

Fig. 8. Individual configurations of the HRP-2 robot extracted from the trajectories above. Note that the IK tend to use many of the degrees of freedom of the body upper part to set the gaze onto the landmark, for example, in the left frame.

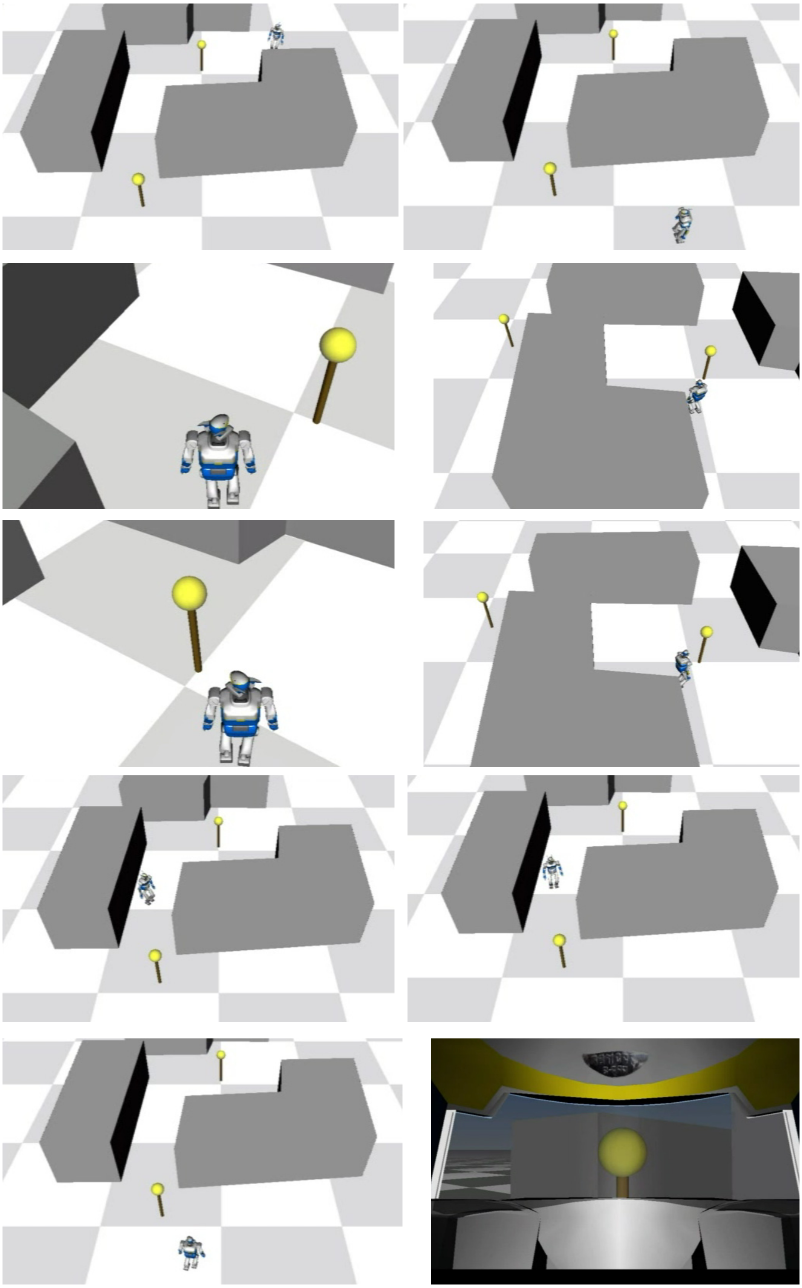

Fig. 9. Two-landmark scenario with obstacles. Top row: initial (left) and final (right) configurations. Second and third rows: the robot surrounds the landmark to execute the path without losing sight of it. Fourth row: the switching moment from viewing the first landmark to viewing the second one. Last row: on the left, a configuration near the end of the path; on the right, a view from the simulated robot camera to the landmark.

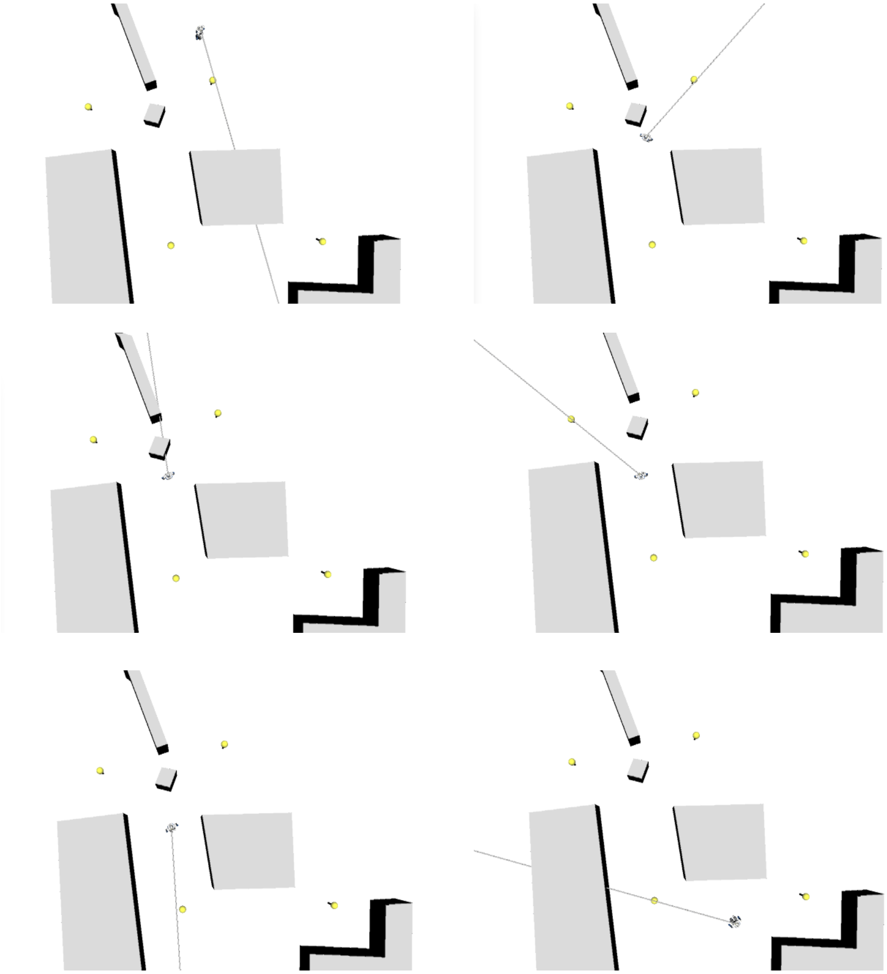

Fig. 10. Top view of a four-landmark scenario with obstacles. Some configurations of the execution of the path. The light ray indicates the gazing direction (the center of the field of view) of the robot to describe which landmark is seen at each shown configuration.

configuration near the end of the path is shown and on the right, an example configuration along the path using the robot view is displayed.

The last simulated scenario, depicted in Fig. 10, describes, from left to right and from top to bottom, the execution of a four-landmark trajectory with obstacles. The light ray on the figure describes the robot's gazing direction, which is the center of the robot field of view. The first and last images show the initial and final configurations on the path. The left figure on the middle row shows the switching point between the first and the second landmark along the trajectory. Here, the field of view is large enough so that the robot can keep in sight the two upper landmarks at the same time. Three landmarks are seen by the robot during the execution of the path.

6.2. *Results with HRP-2*

We ported the planning algorithm on the HRP-2 platform, at the CNRS-AIST Joint French−Japanese Robotics Laboratory in Tsukuba. The tracking system used to enforce the visual constraints is part of the ViSP package.[29]

In our first experiment, illustrated by Fig. 11, we have used a closet fixed on a wall as a unique visual landmark. The same code that we used for the simulations above was used here for generating safe 2D footprints path. Then, we used our pattern generator, described in Sec. 5, to produce a path that ensures all the described constraints on the real robot.

At this stage, small disturbances on the execution of the path are not explicitly considered. Realization of the motion is done using the pattern generator from Ref. 18. The online pattern generator includes a stabilization process to handle small disturbances when the motion is being executed.

Sample configurations during the execution of the path are shown in Fig. 11. The landmark is highlighted using red lines around it. The obstacles are the movable walls (static during each experiment) placed around the environment. In this one-landmark scenario, the robot executes the path by first approaching the obstacle to avoid the obstacles and then making backward steps to arrive to the final configuration, placed on the other side of the wall. Note that a shortest path might have been found by walking on the other side of the wall but the landmark would have been occluded by the obstacle, making a surveillance or a localization task much more difficult.

A second experiment was performed using a two-landmark scenario (Fig. 12). Here, the same closet as before is used as the first landmark and a LCD screen with a pink solid image showing on it is used as the second landmark. Both of these landmarks are shown inside red rectangles in Fig. 12(a). The first landmark can be seen during a large portion of the computed trajectory (see Fig. 12(b)) up to the part when the obstacle in the middle of the environment is passed (Fig. 12, second row). After this part of the environment, the first landmark is occluded and the robot is forced to switch obstacles and look at the LCD screen (Fig. 12, fourth row). On the last row on Fig. 12 are the landmarks from the robot viewpoint. The first image is a configuration where the robot is looking at the first landmark, the second one is a configuration when the robot is switching between the first and the second landmarks and therefore both landmarks are in sight, and the third image is a configuration when the second landmark is in sight.

The major issue for the implementation of both of these experiments lies on the sensitivity to the vision processes. For instance in the first part of the video, the robot is using visual servoing on a model map on the environment. If the robot looses track of the object, because the visibility has been violated, it has to stop and find back the object, which, in some cases, may imply human intervention.

Videos for both of these experiments can be found on http://www.cimat.mx/∼cesteves/VigilantHumanoid/.

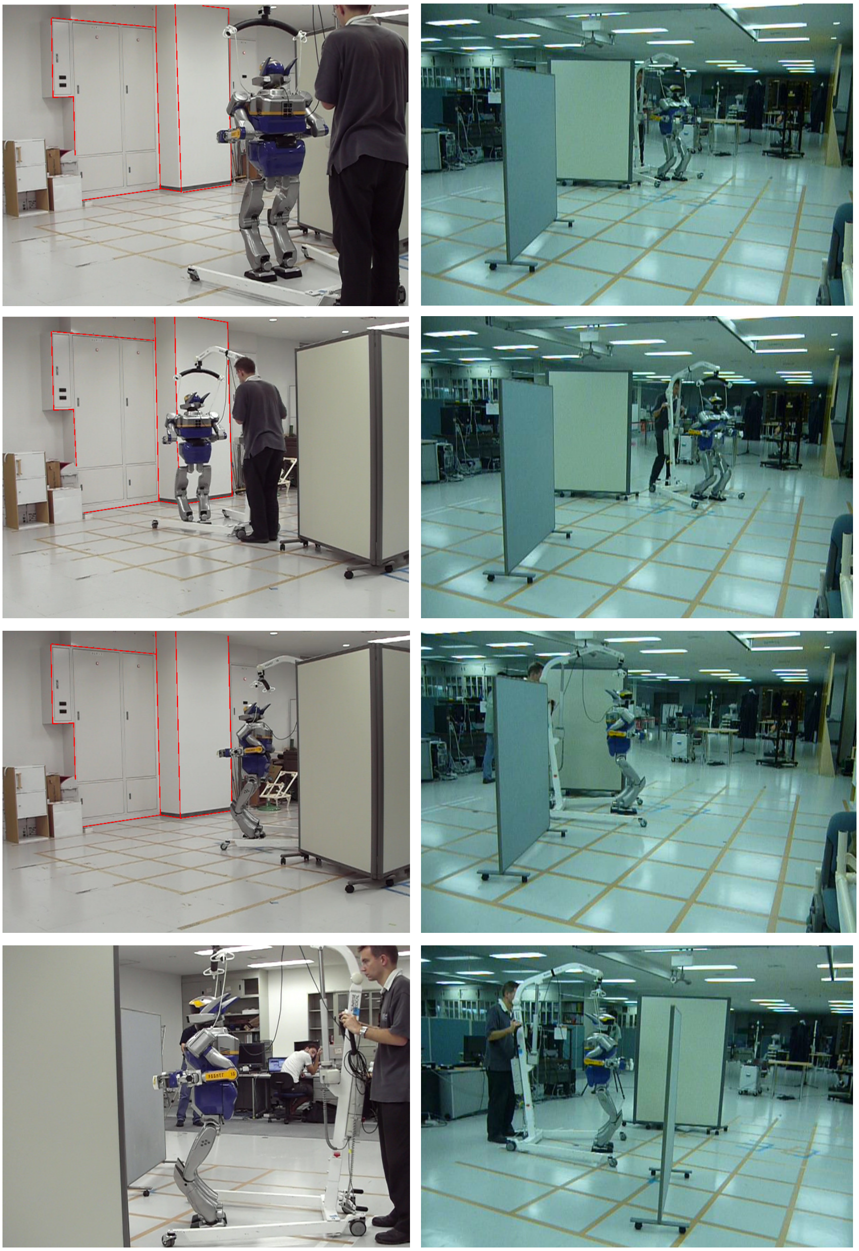

Fig. 11. The execution of a trajectory with obstacles on the HRP-2 robot at four time stamps, from two different points of view.

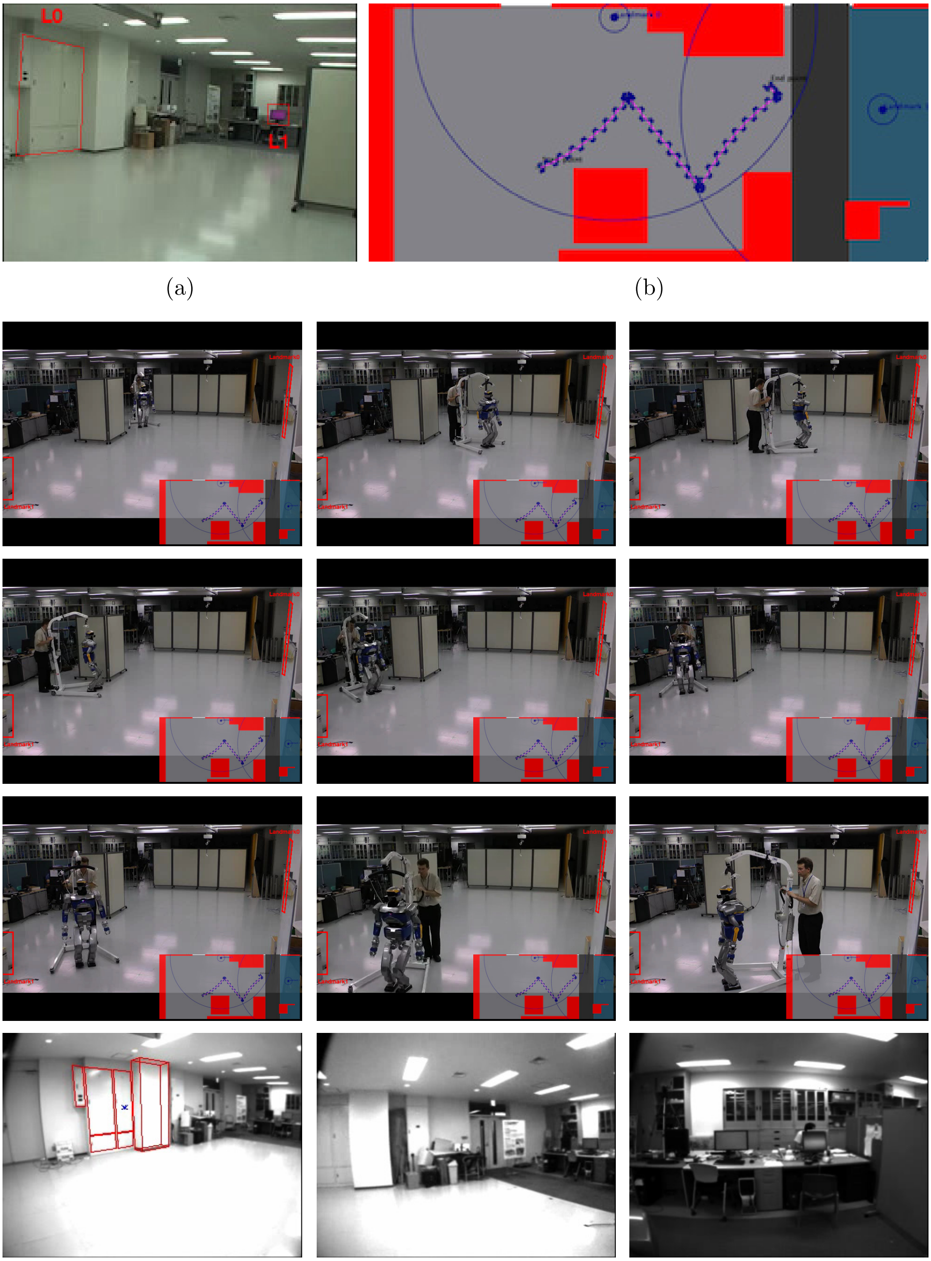

(a)

(b)

Fig. 12. Two-landmark trajectory execution. (a) The landmarks are shown in the image. One is a white closet on the wall and the other is an LCD screen with a pink image. (b) The computed trajectory for two landmarks and a big obstacle in the middle of the room. The rest of the obstacles are on the edges of the room. Second to fourth rows are the execution of the trajectory by HRP-2 robot. Second image on the third row is one of the switching configurations. Fifth row. Left: view from the robot to the first landmark. Middle: view from the robot switching landmarks, at this point both landmarks are in sight. Right: view from the robot to the second landmark, which is the LCD screen from the left.

7. Conclusions and Future Work

We presented an algorithm that allows planning motion for humanoid robots with sensory constraints that are imposed by the presence of one or several landmarks among which at least one must be visible during the whole trajectory. As opposed to most existing approaches, we incorporate these constraints not *a posteriori* but at the planning level with a reduced model of the robot (a DDR), a model to which recent studies within the neuroscience community has given some support. Once a plan has been found for this reduced model, we compute a series of footprints that feed a stack of tasks to generate the humanoid whole-body walking pattern. Chief among the tasks in the stack are the maintenance of the robot stability and a visual servoing task to satisfy all the visibility constraints.

Although our approach generates backward motion that could be considered as unsafe for the robot, we claim that in specific surveillance or localization applications, the algorithm is helpful, as the problem of robot safety can be managed with range sensors. Our approach has been not only tested on simulation examples for the HRP-2 humanoid robot, but also implemented it onboard on the real HRP-2 platform.

Among ongoing and future work, we aim at incorporating more motion primitives to the motion planner for the reduced model. In particular, lateral motions are currently not supported in our scheme but could be helpful in many situations. Approaches such as the one presented in Ref. 30 might be a reasonable solution in our case to include these lateral motions.

Another ongoing work is to consider landmarks not as single points but as polygons, and to ensure that its whole projection, or planar poses, will be kept in sight. This would allow us to perform a visually based control when performing the trajectory, which would be more robust than a position-based trajectory tracking.

References

1. E. Yoshida, J.-P. Laumond, C. Esteves, O. Kanoun, A. Mallet, T. Sakaguchi and K. Yokoi Motion autonomy for humanoids: experiments on hrp-2 no. 14. *Computer Animation and Virtual Worlds* **20**(5–6) (2009) 511–522.
2. J. Chestnutt, J. J. Kuffner, K. Nishiwaki and S. Kagami, Planning biped navigation strategies in complex environments, in *Proceedings of the IEEE-RAS International Conference on Humanoid Robots* (2003).
3. J. Chestnutt and J. J. Kuffner, A tiered planning strategy for biped navigation, in *Proceedings of the IEEE-RAS International Conference on Humanoid Robots* (2004), pp. 422–436.
4. K. Hauser, T. Bretl and J.-C. Latombe, Non-gaited humanoid locomotion planning, in *Proceedings of the IEEE-RAS International Conference on Humanoid Robots* (2005), pp. 7–12.
5. A. Escande and A. Kheddar, Contact planning for acyclic motion with task constraints and experiment on hrp-2 humanoid, in *Proceedings of the IEEE/RSJ International Conference on Intelligent Robots and Systems* (2009), pp. 435–440.
6. E. Yoshida, C. Esteves, I. Belousov, J.-P. Laumond, T. Sakaguchi and K. Yokoi, Planning 3d collision-free dynamic robotic motion through iterative reshaping, *IEEE Transactions on Robotics* **24**(5) (2008) 1186–1198.

7. E. Yoshida, M. Poirier, J.-P. Laumond, O. Kanoun, F. Lamiraux, R. Alami and K. Yokoi, Pivoting based manipulation by a humanoid robot, *Autonomous Robots* **28**(1) 2010 77–88.
8. N. Mansard, O. Khatib and A. Kheddar, A unified approach to integrate unilateral constraints in the stack of tasks, *IEEE Transactions on Robotics* **25**(3) (2009) 670–685.
9. O. Kanoun, F. Lamiraux, P.-B. Wieber, F. Kanehiro, E. Yoshida and J.-P. Laumond. Prioritizing linear equality and inequality systems: Application to local motion planning for redundant robots, in *Proceedings of the IEEE International Conference on Robotics and Automation* (2009), pp. 2939–2944.
10. N. Mansard and F. Chaumette, Task sequencing for high level sensor-based control, *IEEE Transactions on Robotics* **23**(1) (2007) 60–72.
11. Y. Yang and O. Brock, Elastic roadmaps: Globally task-consistent motion for autonomous mobile manipulation in dynamic environments, in *Proceedings of Robotics: Science and Systems* (2006).
12. K. Nishiwaki, J. J. Kuffner, S. Kagami, M. Inaba and H. Inoue, The experimental humanoid robot h7: A research platform for autonomous behaviour, *Philosophical Transactions of the Royal Society* **365** (2007) 79–107.
13. O. Stasse, F. Saïdi, K. Yokoi, B. Verrelst, B. Vanderborght, A. Davison, N. Mansard and C. Esteves, Integrating walking and vision to increase humanoid autonomy, *International Journal of Humanoid Robotics*, 5(2) (2008) 287–310.
14. N. Mansard, O. Stasse, F. Chaumette and K. Yokoi, Visually-guided grasping while walking on a humanoid robot, in *Proceedings of the IEEE International Conference on Robotics and Automation* (2007), pp. 3041–3047.
15. J. B. Hayet, C. Esteves, G. Arechavaleta and E. Yoshida, Motion planning for a vigilant humanoid robot, in *Proceedings of the IEEE-RAS International Conference on Humanoid Robots* (2009), pp. 196–201.
16. H. Hicheur, Q.-C. Pham, G. Arechavaleta, J.-P. Laumond and A. Berthoz, The formation of trajectories during goal-oriented locomotion in humans i: A stereotyped behaviour, *European Journal of Neuroscience* **26**(8) (2007) 2376–2390.
17. G. Arechavaleta, J.-P. Laumond, H. Hicheur and A. Berthoz, On the nonholonomic nature of human locomotion, *Autonomous Robots* **25**(1–2) (2008) 25–35.
18. S. Kajita, F. Kanehiro, K. Kaneko, K. Fujiwara, K. Harada, K. Yokoi and H. Hirukawa, Biped walking pattern generation by using preview control of zero-moment point, in *Proceedings of the IEEE International Conference on Robotics and Automation* (2003), pp. 1620–1626.
19. S. Bhattacharya, R. Murrieta-Cid and S. Hutchinson, Optimal paths for landmark-based navigation by differential-drive vehicles with field-of-view constraints, *IEEE Transactions on Robotics* **23**(1) (2007) 47–59.
20. J. B. Hayet, C. Esteves and R. Murrieta-Cid, A motion planner for maintaining landmark visibility with a differential drive robot, in *Proceedings of the International Workshop on the Algorithmic Foundations of Robotics* (2008), pp. 333–347.
21. P. Salaris, D. Fontanelli, L. Pallottino and A. Bicchi, Shortest paths for a robot with nonholonomic and field-of-view constraints, *IEEE Transactions on Robotics* **26**(2) (2010) 269–281.
22. J.-P. Laumond, P. E. Jacobs, M. Taïx and R. M. Murray, A motion planner for nonholonomic mobile robots, *IEEE Transactions on Robotics and Automation* **10**(5) (1994) 577–593.
23. B. Mirtich and J. Canny, Using skeletons for nonholonomic path planning among obstacles, in *Proceedings of the IEEE International Conference on Robotics and Automation* (1992), pp. 2533–2540.

24. J.-B. Hayet, C. Esteves and R. Murrieta-Cid, Motion planning for maintaining landmarks visibility for a differential drive robot, Submitted to *Robotics and Autonomous Systems*, (2010).
25. B. Siciliano and J.-J. Slotine, A general framework for managing multiple tasks in highly redundant robotic systems, in *Proceedings of the IEEE International Conference Advanced Robotics* (1991), pp. 1211−1216.
26. Y. Nakamura, *Advanced Robotics: Redundancy and Optimization*, (Addison-Wesley Longman Publishing Co., Inc., Boston, MA, USA, 1st edition, 1990.
27. T. Sugihara, Y. Nakamura and H. Inoue, Real time humanoid motion generation through zmp manipulation based on inverted pendulum control, in *Proceedings of the IEEE International Conference on Robotics and Automation* (2002), pp. 1404−1409.
28. F. Kanehiro, H. Hirukawa and S. Kajita, Open hrp: Open architecture humanoid robotics platform, *International Journal of Robotics Research* **23**(2) (2004) 155−165.
29. E. Marchand, F. Spindler and F. Chaumette, Visp for visual servoing: A generic software platform with a wide class of robot control skills, *IEEE Robotics and Automation Magazine* **12**(4) (2005) 40−52.
30. T.-V.-A. Truong, D. Flavigne, J. Pettré, K. Mombaur and J.-P. Laumond, Reactive synthesizing of human locomotion combining nonholonomic and holonomic behaviors, in *Proceedings of the IEEE/RAS-EMBS International Conference on Biomedical Robotics and Biomechatronics* (2010), pp. 632−637.

Jean-Bernard Hayet graduated from ENSTA (Paris), University of Paris 6 and got his Ph.D. from the University of Toulouse (2003) where he worked at CNRS-LAAS. He was a postdoctoral fellow at the University of Liège from 2003 to 2007. Since 2007, he has been working at the Center for Research in Mathematics (CIMAT) in Guanajuato, México. He teaches computer science and his main research interests are in landmark-based navigation, motion planning with perception constraints, and visual tracking.

Claudia Esteves is an associate professor at the Department of mathematics of the University of Guanajuato, México, since September 2007. She received her Ph.D. in Informatic Systems from the University of Toulouse, France, in 2007 where she worked at CNRS-LAAS on the subject on motion planning for humanoid robots and virtual characters. In 2006, she made a short stay with the Joint French−Japanese Robotics Laboratory (JRL) in Tsukuba, Japan, to work on the implementation of motion planning algorithms. Her current research interests are on the motion and task planning of anthropomorphic mechanisms and motion planning with perception constraints.

Gustavo Arechavaleta received his M.S. degree from the Monterrey Institute of Technology and Higher Education (ITESM), México, and his Ph.D. degree from Toulouse University, France, in 2003 and 2007, respectively. During his Ph.D. he was engaged in research on motion planning for anthropomorphic mechanisms and on the computational principles of movement neuroscience via optimal control. Since August 2008, he has been a researcher in the Robotics and Advanced Manufacturing Group at CINVESTAV, México. His current research interests include humanoid motion generation, human locomotion, and trajectory optimization.

Olivier Stasse (*1973) is a senior researcher (CR-1) at CNRS-LAAS, Toulouse. He has been an assistant professor in computer science at the University of Paris 13. He received a Ph.D. in intelligent systems (2000) from the University of Paris 6. His research interests include humanoid robots, and more specifically motion generation motivated by vision. From 2003 to 2011, he was with the Joint French−Japanese Robotics Laboratory (JRL) in Tsukuba, Japan. He has been finalist for the Best Paper Award at ICAR in 2007 and finalist for the Best Video Award at ICRA in 2007, and received the Best Paper Award at ICMA in 2006.

Eiichi Yoshida received M.E. and Ph.D. degrees in precision machinery engineering from Graduate School of Engineering, University of Tokyo, in 1993 and 1996, respectively. In 1996, he joined the former Mechanical Engineering Laboratory, Tsukuba, Japan. He is currently Senior Research Scientist in the Intelligent Systems Research Institute at the National Institute of Advanced Industrial Science and Technology (AIST), Tsukuba, Japan. From 1990 to 1991, he was a visiting research associate at Swiss Federal Institute of Technology in Lausanne (EPFL). He served as Co-Director of AIST/IS-CNRS/ST2I Joint French−Japanese Robotics Laboratory (JRL) at CNRS-LAAS, Toulouse, France, from 2004 to 2008. He is currently Co-Director of CNRS-AIST JRL, UMI3218/CRT, AIST, Japan, since 2009. His research interests include robot task and motion planning, modular robotic systems, and humanoid robots.